2018

Regulation of amyloid-β dynamics and pathology by the circadian clock

Geraldine J. Kress

Fan Liao

Julie Dimitry

Michelle R. Cedeno

Garret A FitzGerald

See next page for additional authors

Authors

Geraldine J. Kress, Fan Liao, Julie Dimitry, Michelle R. Cedeno, Garret A FitzGerald, David M. Holtzman, and Erik S. Musiek

Published Online: 30 January, 2018 | Supp Info: http://doi.org/10.1084/jem.20172347

JEM

Regulation of amyloid-β dynamics and pathology by the circadian clock

Geraldine J. Kress,[1,2] Fan Liao,[1] Julie Dimitry,[1] Michelle R. Cedeno,[1] Garret A. FitzGerald,[4] David M. Holtzman,[1,2,3] and Erik S. Musiek[1,2,3]

[1]Department of Neurology, [2]Hope Center for Neurological Disease, and [3]Knight Alzheimer's Disease Research Center, Washington University School of Medicine, St. Louis, MO
[4]Institute for Translational Medicine and Therapeutics, Perelman School of Medicine, University of Pennsylvania, Philadelphia, PA

Nighttime restlessness and daytime drowsiness are common and early symptoms of Alzheimer's Disease (AD). This symptomology implicates dysfunctional biological timing, yet the role of the circadian system in AD pathogenesis is unknown. To evaluate the role of the circadian clock in amyloid-β (Aβ) dynamics and pathology, we used a mouse model of β-amyloidosis and disrupted circadian clock function either globally or locally in the brain via targeted deletion of the core clock gene *Bmal1*. Our results demonstrate that loss of central circadian rhythms leads to disruption of daily hippocampal interstitial fluid Aβ oscillations and accelerates amyloid plaque accumulation, whereas loss of peripheral *Bmal1* in the brain parenchyma increases expression of *Apoe* and promotes fibrillar plaque deposition. These results provide evidence that both central circadian rhythms and local clock function influence Aβ dynamics and plaque formation and demonstrate mechanisms by which poor circadian hygiene may directly influence AD pathogenesis.

Journal of Experimental Medicine

INTRODUCTION

Loss of normal day/night activity rhythms characterized by increased daytime sleep and nighttime wakefulness is a common symptom of Alzheimer's Disease (AD; Witting et al., 1990; Satlin et al., 1995; Hatfield et al., 2004). These symptoms suggest dysfunctional biological timing in AD, indicative of a faulty circadian system. Accordingly, neuropathological changes in the volume and cell number within the suprachiasmatic nucleus (SCN), the central locus of the circadian system, are observed in postmortem AD tissue and correlate with circadian rhythm degradation (Swaab et al., 1985; Zhou et al., 1995; Harper et al., 2008; Wang et al., 2015). Although circadian dysfunction has long been considered a consequence of AD-related neurodegeneration, it has more recently been hypothesized as a potential contributor to the pathogenesis of AD (Maywood et al., 2006; Hastings and Goedert, 2013; Musiek and Holtzman, 2016). This idea is strongly supported by epidemiological studies showing that a loss of robust circadian activity rhythms or sleep fragmentation in cognitively normal people is associated with increased risk of developing dementia (Tranah et al., 2011; Lim et al., 2013). However, it remains unclear whether or how the circadian system influences AD pathogenesis.

Amyloid plaques composed of aggregated amyloid-β (Aβ) peptides are a defining pathological feature of AD. Identifying factors that influence the accumulation of Aβ peptide is critical toward enhancing our understanding of AD pathogenesis. Normally, soluble Aβ peptide levels exhibit robust daily oscillations in mouse hippocampal interstitial fluid (ISF), as measured by in vivo cerebral microdialysis, as well as in human cerebrospinal fluid (Kang et al., 2009; Huang et al., 2012; Roh et al., 2012). These oscillations show a clear 24-h period, persist in constant dim lighting conditions (Kang et al., 2009), and are in phase with known circadian rhythms in activity, suggesting that Aβ rhythms in the brain may be controlled by the circadian system. Although it is well established that the circadian clock regulates the timing of periods of wakefulness and inactivity as well as many other rhythmic processes in the brain (Toh et al., 2001; Laposky et al., 2005), the role of the circadian system in controlling Aβ dynamics and amyloid plaque deposition remains unknown.

The mammalian circadian system is organized hierarchically, with the central "master" circadian clock in the SCN of the hypothalamus synchronizing subsidiary peripheral clocks distributed throughout the brain and body to coordinate physiology and behavior rhythms within a 24-h period (Mohawk et al., 2012). The central clock in the SCN and peripheral clocks in cells throughout the body use similar core molecular components composed of transcriptional–translational feedback loops to drive clock-controlled gene expression in a tissue-specific manner. At the molecular level, the positive transcriptional limb composed of the transcription factor BMAL1 (also known as aryl hydrocarbon nuclear translocator-like [ARNTL]) in com-

Correspondence to Erik S. Musiek: musieke@wustl.edu

The Rockefeller University Press
J. Exp. Med. 2018 Vol. 215 No. 4 1059–1068
https://doi.org/10.1084/jem.20172347

plex with circadian locomotor output cycles kaput (CLOCK) or neuronal PAS-containing protein 2 (NPAS2) drives circadian transcription of clock-controlled genes including repressor Period (*Per*) and Cryptochrome (*Cry*) genes that comprise the negative regulatory limb of the circadian molecular clock. Deletion of *Bmal1* renders the circadian molecular clock dysfunctional in any given tissue including the SCN, and it prevents clock-mediated transcriptional regulation (Bunger et al., 2000). Mice with global *Bmal1* deletion have complete loss of circadian function both in terms of SCN-driven central rhythms such as activity and temperature as well as cellular transcriptional rhythms across tissues. However, targeted deletion of *Bmal1* within brain regions outside of the SCN disrupts local cellular circadian clock function and gene transcription without disturbing SCN-driven central rhythms (Mieda and Sakurai, 2011; Musiek et al., 2013). Thus, tissue-specific deletion of clock function can be used to evaluate the contribution of peripheral (local) versus central circadian clock function on Aβ dynamics in vivo. In this study, we determine whether the circadian clock controls Aβ oscillations in the hippocampus and impacts amyloid plaque deposition in vivo by using both tissue-specific and global *Bmal1* deletion in a mouse model of β-amyloidosis. Furthermore, we interrogate the relative contributions of the central SCN-driven circadian clock and that of the local clocks of the brain to Aβ dynamics and plaque pathology.

RESULTS AND DISCUSSION

Hippocampus-specific *Bmal1* deletion does not alter ISF Aβ rhythms

Because the circadian clock machinery within the hippocampus can regulate local gene expression, we first sought to determine whether the local hippocampal circadian clock is required for daily oscillations of ISF Aβ by examining the effect of targeted *Bmal1* deletion in the hippocampus in a mouse model of β-amyloidosis. We used the *APPPS1-21* transgenic model, which expresses the human amyloid precursor protein (*APP*) gene bearing the KM670/671NL "Swedish" mutations as well as human presenilin 1 bearing an AD-associated L166P mutation (Radde et al., 2006). We chose this particular AD mouse model because these mice exhibit early onset of amyloid plaques beginning at 2 mo of age. Using young mice (≤4 mo old) eliminates any age-related changes in the mouse's intrinsic circadian system. Also, this AD mouse model is one of the few on a pure C57BL/6 background, thereby minimizing any strain-dependent effects on circadian behaviors. We found that 3–4-mo-old *APPPS1-21* mice do not have any apparent abnormalities in circadian rhythms of behavior or basal clock gene expression (Fig. S1), and thus all circadian dysfunction observed in subsequent experiments was induced by our manipulations of *Bmal1* in this system. Moreover, we observed close correlation between a classical circadian behavior assay involving wheel-running behavior and rhythms in core body temperature, allowing us to use core body temperature for circadian behavioral rhythms in subsequent experiments. To achieve localized deletion of *Bmal1* within the hippocampus, we performed intrahippocampal injection of an adenoassociated virus (AAV8) expressing either Cre–internal ribosome entry site (IRES)-GFP or a GFP control construct in 3-wk-old *APPPS1-21* mice bearing two floxed *Bmal1* alleles (*Bmal1*$^{f/f}$*;APPPS1-21*; Storch et al., 2007). Because amyloid plaque deposition can influence soluble Aβ dynamics (Roh et al., 2012), microdialysis was performed before 2 mo of age, which marks the appearance of amyloid plaque pathology, in all experiments. At 5 wk of age, microdialysis probes were placed directly into the region of viral vector injection, ensuring that *Bmal1* was deleted in the hippocampal tissue directly surrounding the microdialysis probe (Fig. 1, A–D). After a 2-wk recovery from surgery, ISF Aβ levels were measured in freely moving mice for ≤4 d under 12-h:12-h light/dark (L:D) conditions (Kang et al., 2009). Hippocampus-specific *Bmal1* deletion had no effect on the hippocampal daily oscillations of ISF Aβ, suggesting that the local core circadian clock within the hippocampus is not required for daily Aβ oscillations (Fig. 1, E and f).

Bmal1 deletion throughout the brain but with sparing of the SCN leaves ISF Aβ rhythms intact

We next sought to more thoroughly distinguish the effect of peripheral circadian clocks from those of the central clock on ISF Aβ oscillations. Because oscillation in Aβ levels may depend of peripheral circadian clocks in other brain regions that innervate the hippocampus, we examined whether *Bmal1* deletion throughout the entire brain but with sparing of the SCN would impact hippocampal ISF Aβ rhythms. We used *Nestin-Cre*$^{+}$*;Bmal1*$^{(f/f)}$ mice, which have *Bmal1* deleted in neurons and astrocytes throughout the brain but with unperturbed BMAL1 expression in the central clock in the SCN (Fig. 2, A and C). Even with loss of local circadian transcriptional regulation in the cortex and hippocampus, these mice have intact core body temperatures and rest–activity rhythms (Fig. 2, B and D; Musiek et al., 2013). However, we have previously shown that these mice have loss of circadian clock gene transcription in the cerebral cortex and develop astrogliosis because of the loss of local *Bmal1*, effects which are independent of the central clock (Fig. S2 A; Musiek et al., 2013). We examined the effects of brain-specific clock disruption but with intact SCN-mediated rhythms on hippocampal ISF Aβ rhythms by generating *Nestin-Cre*$^{+}$*;Bmal1*$^{f/f}$*;APPPS1-21* mice (referred to as *Nes-Bmal1 KO;APP*). We observed that daily oscillations in hippocampal ISF Aβ in *Nes-Bmal1 KO;APP* mice were similar to those seen in *Cre*$^{-}$*;APP* littermate controls, though the small peak in Aβ levels observed immediately after lights off was slightly blunted (Fig. 2, E and F). These results again show minimal involvement of extra-SCN local cellular clocks of the brain in ISF Aβ rhythms and suggest that these rhythms are mediated by the central clock in the SCN and transmitted to the hippocampus.

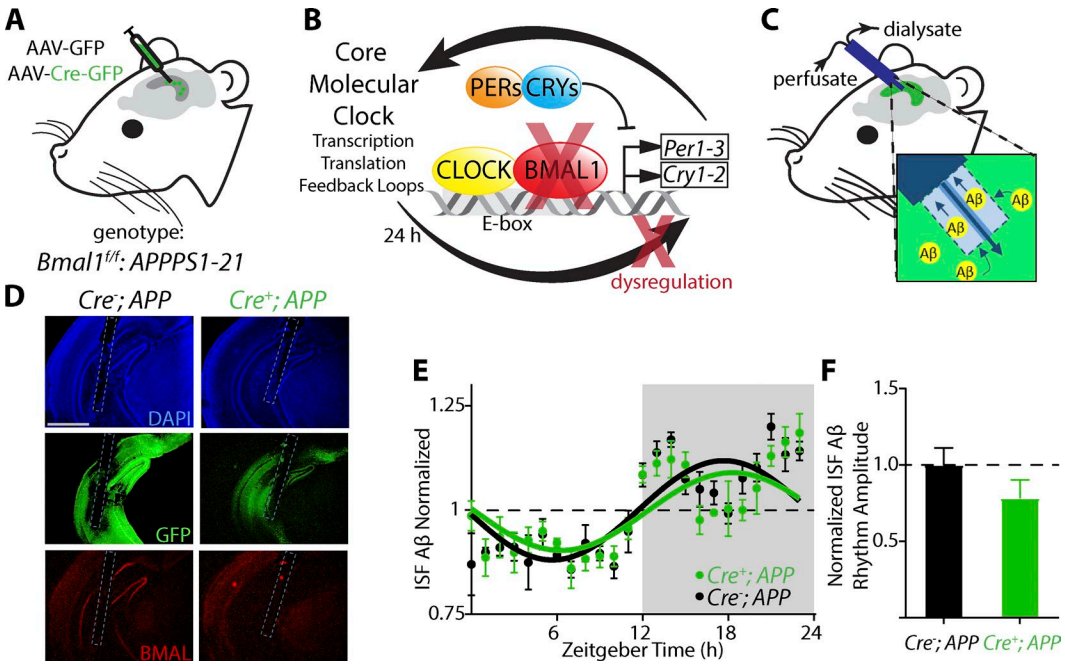

Figure 1. **Intrinsic hippocampal molecular circadian clock function does not influence the daily rhythm of hippocampal ISF Aβ. (A)** Schematic depicting tissue-specific AAV-Cre–mediated excision of *Bmal1* within the hippocampus of *Bmal1*$^{f/f}$*;APPPS1-21* transgenic mice. **(B)** Diagram depicting *Bmal1* deletion abrogating circadian clock function. In addition to *Per* and *Cry* genes, BMAL1 regulates transcription of many other clock-controlled genes in a tissue-specific manner. **(C)** Schematic illustrating the in vivo microdialysis method used to collect soluble Aβ in the hippocampus subsequent to viral injections. This technique was performed in awake, behaving mice. **(D)** Representative images of microdialysis probe placement (dashed lines) within the hippocampus of mice injected with either AAV-GFP (labeled Cre$^-$; APP, left) with normal BMAL1 expression (bottom left) or injected with AAV-Cre–IRES-GFP (labeled Cre$^+$; APP, right), resulting in a loss of local hippocampal BMAL1 expression (bottom right). Bar, 1 mm. **(E)** Graph showing that hourly ISF Aβ levels are not influenced by the targeted hippocampal excision of *Bmal1* (green, AAV-Cre–labeled Cre$^+$; APP) compared with APP mice with normal BMAL1 expression (black, AAV-GFP–labeled Cre$^-$; APP). Dots represent normalized mean hourly ISF Aβ levels in 12-h:12-h L:D conditions (shaded gray) ± SEM (n = 4–5 mice per genotype), and curves represent cosinor method fits. **(F)** Bar graph showing the effect of targeted hippocampal *Bmal1* deletion on the rhythmicity of ISF Aβ as indicated by cosinor circadian amplitudes. Means were NS by two-tailed t test (P = 0.23). Error bars indicate SEM.

Local *Bmal1* deletion in the brain with sparing of the SCN modestly increases fibrillar but not total amyloid plaque burden

We next used *Nes-Bmal1 KO;APP* mice to examine the effect of brain-specific clock disruption but with sparing of the SCN on amyloid plaque pathology. At 4 mo of age, *Cre*$^-$, *Bmal1*$^{(f/f)}$*;APPPS1-21* (*Cre*$^-$*;APP*) mice accumulate mild amyloid plaque pathology in the hippocampus similar to that observed in standard *APPPS1-21* mice. *Nes-Bmal1 KO;APP* littermate mice showed no increase in total amyloid plaque burden within the hippocampus compared with Cre$^-$;*APP* littermates as assessed by $A\beta_{1-13}$ antibody staining (HJ3.4 antibody; Fig. 2, G and H). However, there was a modest but clear trend toward an increase specifically in fibrillar amyloid plaque burden, quantified by staining with the congophilic dye X34, in the hippocampus of *Nes-Bmal1 KO;APP* mice (P = 0.06 by two-tailed t test, and P = 0.03 by one-tailed t test). Thus, mice with deletion of *Bmal1* throughout the extra-SCN brain but with intact central circadian rhythms had relatively normal hippocampal ISF Aβ oscillations, and they showed no change in total plaque levels but did show a small increase in hippocampal fibrillar plaque burden. Collectively, these data indicate that local peripheral clocks do not strongly influence Aβ oscillations or overall plaque deposition in the hippocampus but that local *Bmal1* deletion may promote the formation of fibrillar Aβ plaques.

Global *Bmal1* deletion causes loss of ISF Aβ rhythms in the hippocampus and markedly increases amyloid plaque burden

Finally, we examined the effect of whole-organism circadian disruption, including the SCN, on hippocampal ISF Aβ dynamics and plaque deposition. We were unable to cross *APPPS1-21* mice to standard global *Bmal1 KO* mice because of poor viability. However, we were able to measure endogenous murine ISF Aβ (as opposed to human Aβ in the *APPPS1-21* models) by microdialysis in standard *Bmal1 KO* mice, which have global *Bmal1* deletion and have dysfunctional central and peripheral clocks as well as fragmented activity and core body temperature circadian rhythms (Fig. 3, A and B; Bunger et al., 2000). These experiments allowed us to evaluate the effect of global *Bmal1* deletion on ISF Aβ dynamics, but because there is no human *APPPS1* transgene, the levels of murine Aβ were

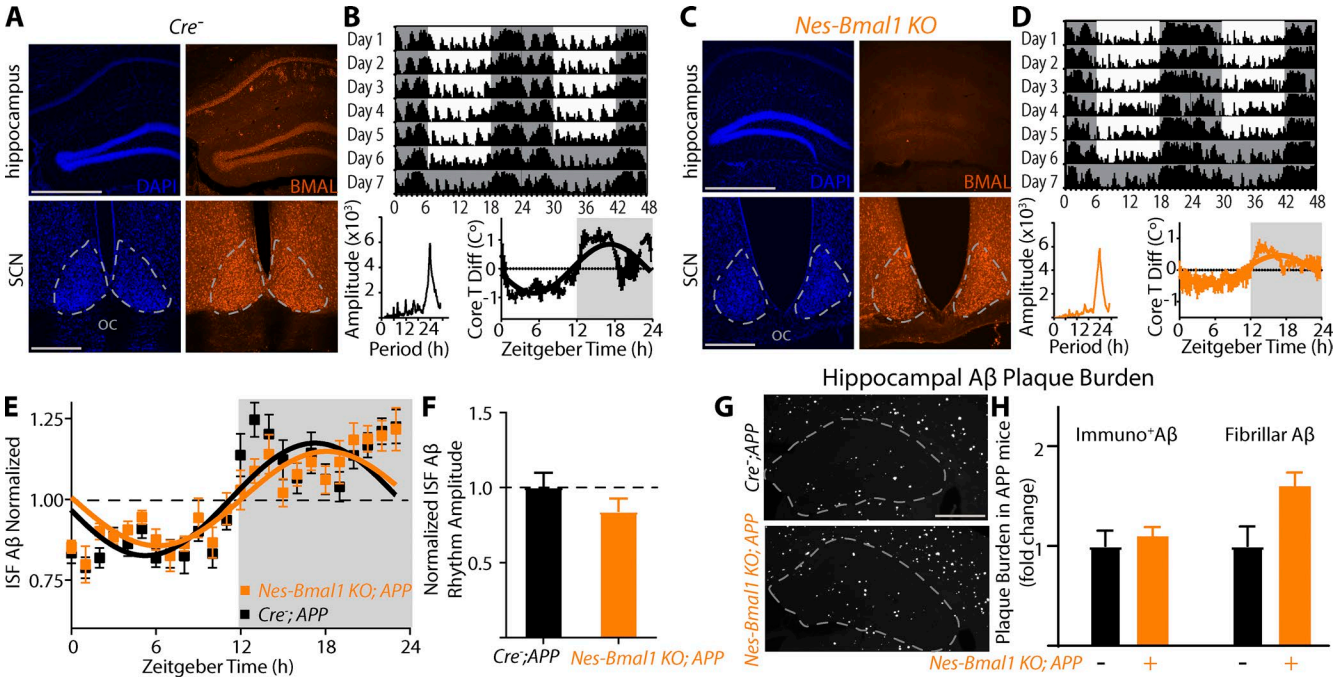

Figure 2. ***Bmal1* deletion throughout in the brain but sparing the SCN does not markedly affect Aβ levels or hippocampal amyloid pathology.** **(A)** Representative images showing normal BMAL1 expression in the hippocampus and SCN regions from a control mouse (*Cre*⁻). **(B)** Representative raw tracing of core body temperature recordings over 7 d from a *Cre*⁻ mouse (top). Mean body core temperature recordings over 6 d in 12-h:12-h L:D (bottom right), with a χ^2 periodogram (bottom left) showing a dominant 24-h rhythm present in a control *Cre*⁻ mouse ($n = 3$). **(C)** Representative images of a *Nestin-Cre*$^+$*;Bmal1*$^{f/f}$ (*Nes-Bmal1 KO*) mouse showing loss of hippocampal but not SCN BMAL1 expression. OC, optic chiasm. **(D)** Representative raw tracing of core body temperature recordings over 7 d from a *Nes-Bmal1 KO* mouse (top). Mean body core temperature recordings over 6 d in 12-h:12-h L:D (bottom right), with a χ^2 periodogram (bottom left) showing a dominant 24-h rhythm present in a *Nes-Bmal1 KO* mouse ($n = 3$). **(E)** Graph showing hourly hippocampal ISF-soluble Aβ levels in *Cre*⁻*;Bmal1*$^{f/f}$*;APPPS1-21* (black) and *Nestin-Cre*$^+$*; Bmal1*$^{f/f}$*;APPPS1-21* (*Nes-Bmal1 KO;APP,* orange) mice. Squares represent the normalized mean hourly ISF Aβ level in 12h:12-h L:D conditions (shaded gray) ± SEM ($n = 5$ mice per genotype), and curves represent cosinor method fits. **(F)** Bar graph showing rhythmicity of ISF Aβ as indicated by cosinor circadian amplitudes in *Cre*⁻*;APPPS1-21* (black) and *Nes-Bmal1 KO;APP* (orange) mice. Means were NS by two-tailed *t* test (P = 0.26). **(G)** Representative images showing X34 staining of fibrillar Aβ plaques in the hippocampus of 4-mo *Cre*⁻*;APPPS1-21* (top) and *Nes-Bmal1 KO;APP* mice (bottom). The hippocampus is outlined by dashed gray lines. Bars: (A and C, top, and G) 500 µm; (A and C, bottom) 250 µm. **(H)** Bar graph showing quantification of immunoreactive Aβ (HJ3.4 antibody staining, left) and fibrillar Aβ (X34 staining, right) plaque burden within the hippocampus of *Cre*⁻*APPPS1-21* (black) and *Nes-Bmal1 KO;APP* (orange) mice ($n = 9$–14 mice per genotype). Bars represent means ± SEM (two-tailed *t* test; P = 0.88 for the immunoreactive Aβ comparison, and P = 0.064 for the fibrillar Aβ comparison).

lower, and samples had to be pooled to detect Aβ, decreasing the sampling frequency. Despite these obstacles, we found that arrhythmic *Bmal1 KO* mice had severely diminished daily oscillations in hippocampal ISF Aβ, even under 12-h:12-h L:D conditions, as compared with WT littermates (Fig. 3 C). Aβ oscillation amplitude was significantly decreased by 50% in global *Bmal1 KO* mice (Fig. 3 D). However, integrated levels of ISF Aβ over the 24-h circadian cycle were similar to WT littermate controls (Fig. 3 E), demonstrating that although *Bmal1* deletion disrupts the day/night rhythms of Aβ (leading to higher levels during the light period and lower levels during the dark), it does not cause gross increases in Aβ levels. Thus, loss of central and peripheral rhythms caused by global *Bmal1* deletion abrogates rhythmicity of ISF Aβ in the hippocampus.

Because standard global *Bmal1 KO;APPPS1-21* mice were not viable in our hands and because mice do not develop amyloid plaques without a human APP transgene, we chose to examine the effects of global *Bmal1* deletion on amyloid plaque deposition using a tamoxifen-inducible global *Bmal1 KO* mouse (*CAG-Cre*^{ERT2}*;Bmal1*$^{f/f}$, abbreviated as *Bmal1 iKO*), which could be bred onto an *APPPS1-21* background. *Bmal1 iKO* mice were previously characterized and phenocopy standard *Bmal1* KO mice as they become transcriptionally arrhythmic after tamoxifen treatment and develop astrogliosis (Yang et al., 2016). Indeed, tamoxifen treatment of *Bmal1 iKO* mice at 8 wk of age resulted in a nearly complete deletion of BMAL1 throughout the brain, including the SCN (Fig. 4, A and C), and led to a loss of circadian core body temperature rhythms (Fig. 4, B and D). However, postnatal deletion of *Bmal1* in these mice avoids the developmental pathologies and early mortality observed in standard *Bmal1 KO* mice (Yang et al., 2016). We generated *CAG-Cre*^{ERT2}*;Bmal1*$^{f/f}$*;APPPS1-21* mice (abbreviated as *Bmal1 iKO;APP*) to evaluate the effect of circadian disruption

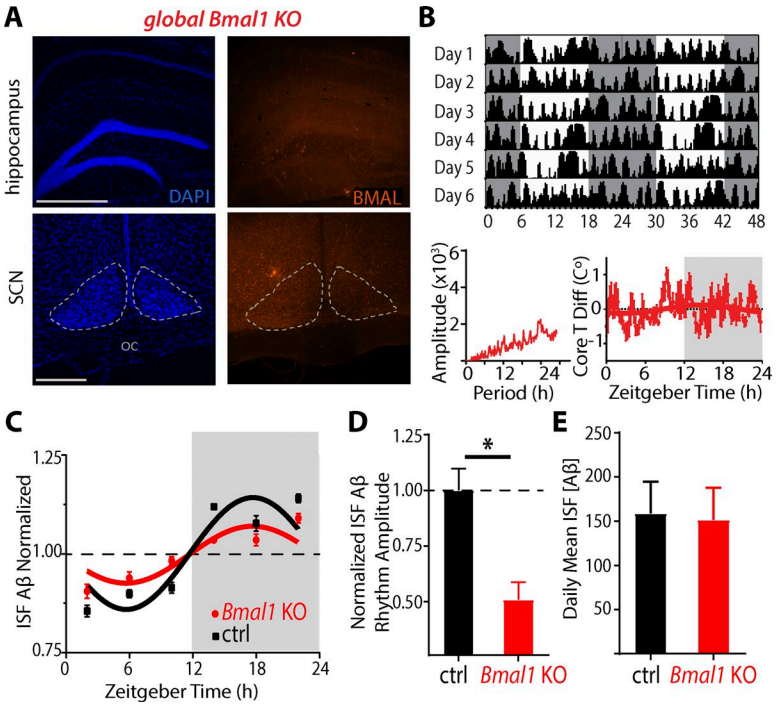

Figure 3. **Global *Bmal1* deletion disrupts Aβ rhythmicity. (A)** Representative images showing decreased BMAL1 expression in the hippocampus and SCN regions from a global *Bmal1 KO* mouse. **(B)** Representative raw tracing of core body temperature recordings over 6 d from a *Bmal1 KO* mouse. Mean body core temperature recordings over 6 d in 12-h:12-h L:D (bottom right), with a χ^2 periodogram (bottom left) showing a loss of the dominant 24-h rhythm in a global *Bmal1 KO* mouse (n = 3). **(C)** Graph showing hippocampal ISF-soluble Aβ levels in WT (labeled control, black) and global *Bmal1 KO* mice (red). Squares represent the normalized mean murine ISF Aβ level pooled every 3 h in 12h:12-h L:D conditions (shaded gray) ± SEM (n = 7 mice per genotype), and curves represent cosinor method fits. **(D)** Bar graph showing rhythmicity of ISF Aβ as indicated by cosinor circadian amplitudes in WT (labeled control, black) and *Bmal1 KO* (red) mice. *, P = 0.002 by two-tailed t test. **(E)** Bar graph depicting daily mean hippocampal ISF Aβ levels in WT (black) and *Bmal1 KO* mice (red). Means were NS by two-tailed t test (P = 0.71). Means + SEM are shown; n = 7 mice/group.

on amyloid plaque deposition. Notably, *Bmal1 iKO;APP* mice were not amenable to ISF Aβ measurement as the tamoxifen regimen was toxic to mice <6 wk old and treatment after that age did not allow sufficient time to allow for surgery, recovery, and microdialysis before plaque accumulation had begun at 2 mo of age. We treated cohorts of *Bmal1 iKO;APP* mice and their Cre⁻ littermate controls (*Bmal1$^{f/f}$;APPPS1-21* mice; both sexes) with tamoxifen for 5 d starting at 8 wk of age and collected tissues at 4 mo of age. *Bmal1 iKO:APP* mice accumulated significantly more hippocampal amyloid plaque burden, quantified either by Aβ antibody to assess total plaque load or by staining with the congophilic dye X34 to assess fibrillar plaque pathology (Fig. 4, E and F). Thus, global disruption of circadian function by postnatal global *Bmal1* deletion increases amyloid plaque deposition in the hippocampus. Collectively, our results show that global *Bmal1* deletion abolishes behavior rhythms mediated by the central clock, disrupts local clock-mediated transcription, abrogates ISF Aβ rhythms, and increases amyloid plaque deposition in the hippocampus.

Bmal1 regulates local apolipoprotein E (*Apoe*) expression in the brain

To explore possible transcriptional mechanisms by which the circadian system regulates Aβ plaque deposition, we performed transcriptional analysis of a panel of genes with known functions related to Aβ production, clearance, or aggregation in cortex tissue from *Nes-Bmal1 KO* (which have intact central rhythms but local *Bmal1* deletion) and *Bmal1 iKO* mice (which have disrupted central rhythms and local *Bmal1* deletion) as well as *Cre*⁻ controls. Expression of several Aβ-related genes were altered, and these changes were generally consistent between the two models, suggesting local transcriptional regulation by *Bmal1* (Fig. S2 A). Among these, we observed significantly increased expression of *Apoe* in both mouse models, demonstrating that *Apoe* is regulated by local BMAL1 independent of the central clock. We examined *Apoe* expression in cortex tissue from *Cre*⁻ controls and *Nes-Bmal1 KO* mice across the circadian cycle. *Apoe* mRNA showed only a modest time-of-day variation in control mice and was increased at all time points in *Nes-Bmal1 KO* mice (Fig. S2 B). The human APOE genotype is major determinant of AD risk, and murine *Apoe* has been shown to potently promote amyloid plaque deposition, specifically fibrillar amyloid plaques (Holtzman et al., 2000; Fagan et al., 2002; DeMattos et al., 2004; Kim et al., 2011). Thus, local *Bmal1* deletion in the brain induces *Apoe* expression, providing one potential mechanism by which local *Bmal1* deletion promotes fibrillar plaque formation. However, multiple BMAL1-controlled pathways may also contribute to this effect.

Our data demonstrate that the circadian system influences daily oscillations in hippocampal ISF Aβ and that disruption of circadian function promotes hippocampal amyloid plaque deposition in vivo. ISF Aβ oscillations do not require local cellular clock function in the hippocampus itself nor in other non-SCN brain regions but instead appear to depend on the central circadian clock within the SCN. Loss of local BMAL1 expression in the hippocampus with sparing of central rhythms in *Nes-Bmal1KO; APP* mice had minimal impact on overall amyloid plaque deposition, but it did promote fibrillar plaque accumulation, perhaps at least in part through direct regulation of *Apoe*. Global *Bmal1-iKO;APP* mice,

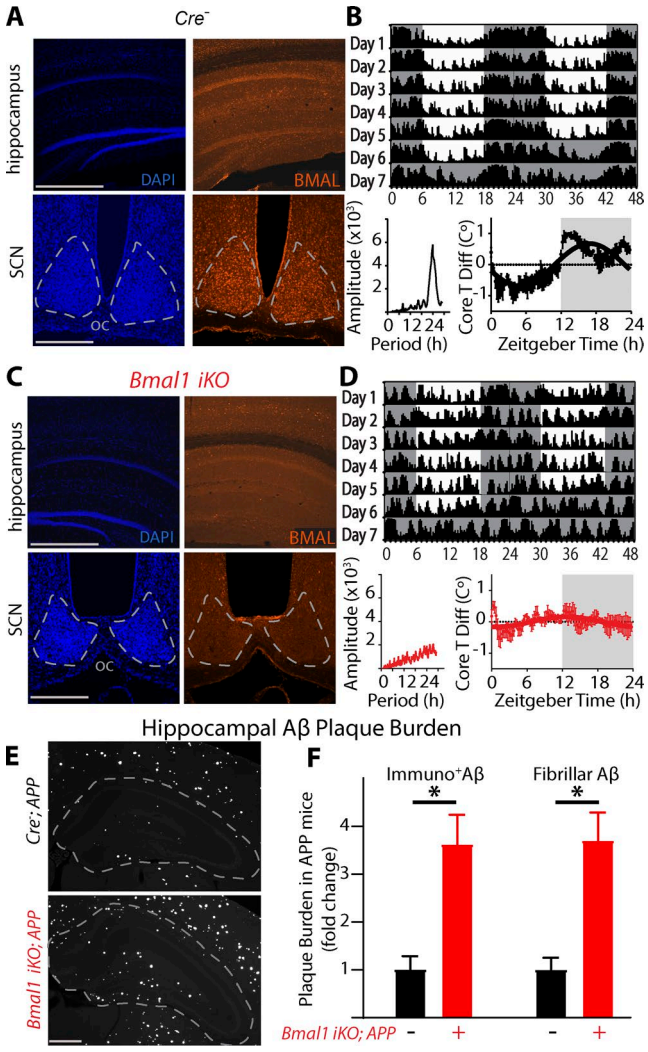

Figure 4. **Global *Bmal1* deletion accelerates amyloid plaque deposition. (A)** Representative images showing normal BMAL1 expression in the hippocampus and SCN regions from a tamoxifen-treated *Cre*⁻ mouse. **(B)** Representative raw tracing of core body temperature recordings over 7 d from a *Cre*⁻ mouse (top). Mean body core temperature recordings over 6 d in 12-h:12-h L:D (bottom right), with a χ^2 periodogram (bottom left) showing a dominant 24-h rhythm present in a *Cre*- control mouse (n = 3). **(C)** Representative images of a tamoxifen-treated *CAG-Cre*$^{ERT2+}$;*Bmal1*$^{f/f}$ (*Bmal1 iKO*) mouse showing a loss of both hippocampal and SCN BMAL1 expression. OC, optic chiasm. **(D)** Representative raw tracing of core body temperature recordings over 7 d from an inducible *Bmal1 KO* mouse (top). Mean body core temperature recordings over 6 d in 12-h:12-h L:D are arrhythmic (bottom right), with a χ^2 periodogram (bottom left) showing a loss of the dominant 24-h rhythm (n = 3). **(E)** Representative images showing X34 staining of fibrillar Aβ plaques in the hippocampus of 4-mo *Cre*⁻;*Bmal1*$^{f/f}$;*APP* (*Cre*⁻;*APP*, top) and *Bmal1 iKO;APP* (red) mice (bottom). The hippocampus is outlined by dashed gray lines. Bars: (A and C, top, and E) 500 µm; (A and C, bottom) 300 µm. **(F)** Bar graph showing quantification of immunoreactive Aβ (HJ3.4 antibody staining, left) and fibrillar Aβ (X34 staining, right) plaque burden within the hippocampus of *Cre*⁻;*APP* (black) and *Bmal1 iKO;APP* (red) mice (n = 8–13 mice per genotype). Bars represent means ± SEM (two-tailed t test; P = 0.001 for the immunoreactive Aβ comparison, and P = 0.001 for the fibrillar Aβ comparison). *, P < 0.05.

which have an arrhythmic central clock and local *Bmal1* deletion, develop much more striking increases in plaque burden than *Nes-Bmal1KO; APP* mice, which have normal central rhythms but local *Bmal1* deletion, showing that the increases in amyloid pathology cannot be fully explained by noncircadian effects of *Bmal1* deletion and are likely caused by a combination of dysregulated SCN-mediated circadian control of Aβ oscillations and local alterations in BMAL1-mediated transcription. In total, our study suggests that the circadian system is critical for maintaining proper Aβ oscillations and Aβ homeostasis in the hippocampus and that circadian dysfunction may disrupt the normal temporal synchrony or feedback inhibition between Aβ production and systems involved in Aβ clearance and/or aggregation. As circadian rhythm dysfunction appears to precede cognitive impairment in AD (Tranah et al., 2011; Musiek et al., 2018), our findings highlight novel mechanisms linking early circadian dysfunction to accelerated amyloid plaque accumulation and provide evidence for an important influence of the circadian system on AD pathogenesis.

Fragmented circadian rhythms can be detected in normal aging as well as in preclinical AD (Musiek et al., 2018) and become more apparent in early symptomatic AD (Hatfield et al., 2004; Harper et al., 2005). Degeneration of the SCN has been described in AD and linked to circadian rhythm degradation (Swaab et al., 1985; Zhou et al., 1995; Harper et al., 2008; Wang et al., 2015). Altered *Bmal1* expression or function has also been specifically associated with AD. Altered methylation of *Bmal1* in AD has been proposed as a possible cause of circadian dysfunction (Cronin et al., 2017), whereas Aβ can reportedly induce BMAL1 degradation in an AD mouse model (Song et al., 2015). Finally, polymorphisms in *Bmal1* are associated with increased AD risk in ApoE4-negative individuals (Chen et al., 2015). Thus, there is a strong biological rationale for modeling AD-related circadian dysfunction by disrupting *Bmal1*. However, *Bmal1* regulates expression of transcripts which are nonrhythmic, suggesting that it serves noncircadian functions (Yu and Weaver, 2011; Yang et al., 2016). We have previously demonstrated that *Bmal1* deletion can induce glial activation and oxidative damage in *Nes-Bmal1 KO* mice, which have normal circadian rhythms and sleep timing, demonstrating that *Bmal1* can exert critical local effects in the brain (Musiek et al., 2013). However, in this study, we did not see significant effects of local *Bmal1* deletion on ISF Aβ dynamics or total plaque deposition, demonstrating that the effects of global *Bmal1* deletion on hippocampal ISF Aβ and plaque burden are at least in part a result of disrupted central rhythms. Increased *Apoe* expression was observed in both *Nes-Bmal1 KO* and *Bmal1 iKO* mice, suggesting that loss of *Bmal1* induces local *Apoe* expression independent of an effect on rhythms or sleep. It has been well established that APOE specifically promotes fibrillar amyloid plaque deposition, as *APP* transgenic mice lacking *Apoe* have striking decreases in fibrillar plaque burden (Holtzman et al., 2000; Fagan et al., 2002; DeMattos et al., 2004; Kim et al., 2011).

Thus, the local tissue effect of *Bmal1* deletion on *Apoe* levels could potentially explain the specific increase in fibrillar plaques in *Nes-Bmal1 KO;APP mice*. However, our data suggest that the combination of central clock dysfunction, which disrupts ISF Aβ rhythms, and local *Bmal1* deletion, which increases local *Apoe* expression and may alter other pathways, leads to a striking increase in plaques observed in *Bmal1 iKO;APP* mice (see Fig. 4).

It is well established that sleep exerts a powerful influence on Aβ plaque pathology as sleep deprivation accelerates plaque deposition, whereas increasing sleep through inhibition of orexin signaling mitigates plaque accumulation (Kang et al., 2009; Roh et al., 2014). The central circadian clock of the SCN regulates the timing of sleep and thus could affect amyloid plaque deposition through a sleep-dependent mechanism. Our data show that this may be the case as *Bmal1 iKO* mice, which have fragmented sleep rhythms, have a greater increase in plaques than SCN-sparing brain-specific *Nes-Bmal1 KO* mice, which have normal sleep timing. However, this is not caused by sleep deprivation as global *Bmal1 KO* mice are known to have slightly increased total and slow-wave sleep (Laposky et al., 2005). *Bmal1 KO* mice do have arrhythmic sleep timing with loss of variation in sleep between the light and dark periods (Laposky et al., 2005), a pattern which resembles the sleep and wake fragmentation observed in AD patients, who often wake throughout the night and nap throughout the day (Witting et al., 1990; Satlin et al., 1995; Hatfield et al., 2004). This circadian fragmentation appears before symptom onset in AD (Tranah et al., 2011; Musiek et al., 2018), suggesting that it could exacerbate amyloid deposition in an early phase of AD pathogenesis. A clear implication of our findings is that therapies directly targeting the circadian system to normalize circadian timing, rather than just augmenting total sleep, may be beneficial in the prevention of AD.

Our study has some limitations. Our microdialysis experiments were performed in standard 12-h:12-h L:D conditions rather than constant darkness. Because *Bmal1 iKO;APP* mice developed increased plaques in L:D conditions, we concluded that it was critical to demonstrate that ISF Aβ oscillations were also disturbed in L:D, which is what we observed. Moreover, *Bmal1* deletion causes arrhythmicity even in L:D conditions, making repetition of these experiments in constant darkness less critical. Direct lesioning of the SCN in *APPPS1-21* mice to disrupt central rhythms without deleting local clock genes would provide complementary data to our study, though such experiments are fraught with difficulty as the SCN is small and surrounded by other hypothalamic nuclei, which can potentially also impact amyloid plaque development if accidently damaged. These studies could be pursued in the future. Monitoring of sleep by electroencephalography was not performed, though electroencephalography analysis of sleep has previously been performed in standard *Bmal1 KO* and *Nes-Bmal1 KO* mice and was found to be arrhythmic in the former and normal in the latter and correlated closely with actigraphy and body temperature rhythms in both models.

In summary, our data reveal the importance of circadian timing in the regulation of amyloid pathology. The circadian system orchestrates the synchrony between many physiological processes with the external environment and regulates gene transcription in various cell types throughout the brain. Our findings demonstrate a potential mechanistic link between circadian dysfunction and AD pathogenesis, suggesting that therapeutic efforts to optimize circadian timing may hold promise for AD prevention.

MATERIAL AND METHODS

Reagents and animals

The following antibodies were used: BMAL1 rabbit polyclonal (1:2,000; 2288; Novus Biologicals) and a monoclonal $A\beta_{1–13}$ (1:1,000; HJ3.4) made in-house (Kang et al., 2009). Various salts and BSA were purchased from Sigma-Aldrich. Mice with germline deletion of *Bmal1* (*Bmal1*$^{-/-}$), *Nestin-Cre*$^{+}$ (stock 03771), *CAG*^{ERT2}*-Cre*$^{+}$ (stock 004453), and *Bmal1*$^{f/f}$ (stock 07668) mice were purchased from The Jackson Laboratory. *APPPS1-21* mice were obtained from M. Jucker (University of Tübingen, Tübingen, Germany). *Bmal1*$^{f/f}$ or *Bmal1*$^{f/f}$*:APPPS1-21* mice were crossed with either tamoxifen-inducible universal (*CAG-Cre*^{ERT2}) mice or with *Nestin-Cre*$^{+/–}$ mice to yield *Bmal1*$^{f/f}$ mice without *Cre, Bmal1*$^{f/f}$*: CAG-Cre*$^{ERT2+/–}$ mice, and *Bmal1*$^{f/f}$*;Nestin-Cre*$^{+/–}$ mice with or without a single copy of the *APPPS1–21* transgene. All mice were maintained on a C57Bl6 background. Both genders were used in all experiments. Mice were bred and housed in accordance with Washington University Animal Studies committee protocols. Mice were bred and group housed (unless otherwise stated) under 12-h:12-h L:D conditions with ad libitum access to food and water. Tamoxifen stock solution (25 mg/ml;T5648; Sigma-Aldrich) was prepared as previously described (Yang et al., 2012) and administered to 2-mo-old *Bmal1*$^{f/f}$*;Cre*$^{ERT2-}$*;APP PS1-21* mice seven times over 5 consecutive days at 100 µl per dose by oral gavage. The efficacy of *Bmal1* excision 2 mo after the tamoxifen regimen was assessed by the levels of quantitative PCR (qPCR) transcripts and BMAL1 immunostaining within the hippocampus. Mice with a reduction of at least 75% BMAL1 immunoreactivity within the hippocampus or an at least 50% reduction in mRNA of *Dbp*, a BMAL1-controlled gene, met the criteria for further analysis. For circadian gene expression experiments, mice were housed in constant darkness for 24 h before and throughout harvest and were anesthetized in darkness before perfusion. Mice were perfused at 4-h intervals starting at 6:00 AM and ending 24 h later.

Stereotaxic injections

Stereotaxic guided surgeries were performed on isoflurane-anesthetized mice as previously described (Kress et al., 2013). In brief, AAV8 vectors expressing Cre-IRES-GFP or just GFP under the chicken β-actin promoter (AAV8-CBA-Cre-IRES-GFP or AAV8-CBA-GFP) were prepared by the

Washington University Viral Vector Hope Center Core and injected unilaterally into the hippocampus of 3-wk-old *Bmal1*$^{f/f}$*:APPPS1-21* mice (2 µl at 1e13 titer level). Successful targeting produced fluorescence primarily in the hippocampus and focal *Bmal1* excision within the hippocampus and was confirmed by the lack of BMAL1 immunoreactive hippocampal tissue at the termination of the experiment. Mice recovered for 3 wk before undergoing microdialysis cannula implantation.

Microdialysis

Hippocampal in vivo Aβ microdialysis was performed as previously described (Kang et al., 2009; Roh et al., 2012). At ∼6 wk of age, AAV-injected *Bmal1*$^{f/f}$*:APPPS1-21*, *Bmal1*$^{f/f}$*:Nestin-Cre*$^{+/-}$*:APPPS1-21*, or germline *Bmal1* KO mice (∼2–3 mo old) were implanted with a guide cannula for microdialysis in the left hippocampus (bregma, 3.1 mm, 2.5 mm lateral to midline, and 1.2 mm below the dura at a 12° angle) and recovered in their home cage for ∼2 wk. On the day microdialysis began, mice were tethered to a Basi Raturn System, and a microdialysis probe (2 mm; 38-kD molecular weight cutoff; BR style; BioAnalytical Systems) was inserted into the left hippocampus through the guide cannula and connected to a syringe pump (Stoelting). Artificial cerebrospinal fluid, pH 7.35, containing 1.3 mM $CaCl_2$, 1.2 mM $MgSO_4$, 3 mM KCl, 0.4 mM KH_2PO_4, 25 mM $NaHCO_3$, 122 mM NaCl, and 0.15% BSA was continuously perfused through the microdialysis probe at a constant flow rate of 1 µl/min (for the detection of murine Aβ, the flow rate was adjusted to 0.5 µl/min). After 3 d of habituation, hourly microdialysis samples were collected over 2–4 d (Cirrito et al., 2003; Kang et al., 2009). The mean daily ISF Aβ level was calculated over 2–3 d for each mouse. The rhythm amplitude of the daily ISF Aβ oscillation was determined using the circadian cosinor method (circadian.org/softwar.html). Data from probe placements outside of the hippocampal region or from mice that did not eat, drink, or move normally were discarded.

Circadian temperature rhythm

Thermochron iButtons (DS1921H) were used to continually record core body temperature rhythms every 15 min as previously described (Pilz et al., 2015). In brief, in anesthetized mice, a longitudinal abdominal incision was made, and the iButton was positioned within the intraperitoneal cavity. Incisions were closed with absorbable and nylon sutures. Mice were house individually in 12-h:12-h L:D conditions for 3–4 wk and then for 2–7 d in constant dark (DD) conditions before the retrieval of the iButton. Temperature values were imported into ClockLab Analysis (6.0.35; Actimetrics) to create actograms and L:D periodograms (χ^2 method).

ELISA

Microdialysis samples were analyzed for Aβx-40 with a sandwich ELISA (Roh et al., 2012). In brief, a monoclonal Aβ antibody targeted against amino acids 35–40 (HJ2) was used to capture Aβx-40 peptide. A biotinylated central domain monoclonal antibody was then applied (HJ5.1). Assays were developed using Super Slow ELISA TMB after an incubation with streptavidin–poly-HRP40 (Fitzgerald). A Bio-Tek Synergy 2 plate reader was used to read the optical density at 650 nm. Samples were run in replicate, and replicates with a coefficient of variation >15% were discarded.

qPCR

For RNA isolation, frozen cortical tissue was homogenized in TRIzol (Invitrogen). Chloroform (1:5) was added, samples were agitated and centrifuged at 13,000 *g* for 15 min at 4°C, and then the chloroform layer was removed, diluted 1:1 in 70% ethanol, and purified using RNA purification columns and reagents (PureLink; Thermo Fisher Scientific). RNA was converted to complementary DNA via reverse transcription using the High-Capacity cDNA-RT kit (MultiScribe; Applied Biosystems) with 1 µg RNA per 20 µl reaction. Quantitative real-time PCR was then performed using proprietary TaqMan primers and reagents and an ABI StepOne qPCR machine (Thermo Fisher Scientific). All mRNA levels were normalized to β-actin (*Actb*) mRNA levels.

Immunohistochemistry

Immunostaining was performed as previously described (Roh et al., 2012). In brief, mice were deeply anesthetized via i.p. pentobarbital followed by transcardial perfusion with ice-cold PBS containing 3,000 U/liter heparin for 3 min. The whole brain or only one hemisphere was fixed in 4% paraformaldehyde for 24 h (4°C) and then cryoprotected with 30% sucrose in PBS (4°C) for 48 h, and 50-µm serial coronal sections were cut on a freezing sliding microtome. For antibody staining, sections were incubated in PBS for 30 min at RT before blocking for 30 min in PBS containing 3% goat serum, 2% BSA, and 0.25% Triton X-100, and then they were incubated overnight in PBS plus 0.10% Triton X-100 with primary antibody and 1% goat serum at 4°C. Sections were then washed with PBS containing 0.1% Triton X-100 for 30 min followed by a 1-h RT incubation with fluorophore-conjugated secondary antibody (Alexa Fluor 488– or 568–conjugated anti–rabbit or anti–mouse) and then washed. Nuclei were visualized with DAPI (Invitrogen) in PBS for 30 min at RT, and then sections were washed for 15 min in PBS and mounted on a coverslip using either Fluoromount (Sigma-Aldrich) or ProLong Gold Antifade Mountant (Invitrogen). For X34 staining, sections were washed in PBS plus 0.10% Triton X-100 for 30 min and then incubated in staining media containing 60% PBS (vol/vol), 40% ethanol, 1:500 volume of 10 N NaOH, and 10 µM X34 for 20 min at RT. Sections were then washed for three time for 2 min each in 60% PBS (vol/vol) and 40% ethanol solution and then washed twice for 5 min each in PBS plus 0.10% Triton X-100. HJ3.4-stained sections were incubated with biotinylated secondary antibodies (Cell Signaling Technologies) and then with streptavin-conjugated horseradish peroxidase (ABC kit; Vector Labs), and then were visualized with diaminobenzidine (Sigma-Aldrich). Sections were then

imaged with either an Eclipse 80i microscope (Nikon) with an Orca-Flash camera (4.0; Hamamatsu Photonics) using a MetaMorph (Molecular Devices) system or an A1Rs1 confocal system (Nikon; Washington University Center for Cellular Imaging). Images were adjusted in ImageJ (National Institutes of Health) or Photoshop (Adobe) for brightness, contrast, and pseudocoloring.

Plaque burden quantification

For plaque burden quantification, serial coronal sections (50 µm thick) were collected from the corpus callosum to caudal hippocampus. Approximately 3–4 sections (each separated by 300 µm) were stained with biotinylated HJ3.4 antibody to visualize Aβ-immunoreactive plaques or X34 dye to visualize fibrillar amyloid plaques. Sections were then imaged with either an Eclipse 80i microscope with an Orca-Flash 4.0 using the MetaMorph system or an Axioscan Z1 automated slide scanning system (ZEISS; Washington University Center for Cellular Imaging). Using a neurostereological method as described previously (Kang et al., 2009), the percent area covered within the hippocampus by HJ3.4 or X34-positive staining was calculated using ImageJ software. Sections from a full set of mice for a given experiment were stained together as a batch, and imaging parameters were held constant across all sections.

Data analysis and statistics

Graphical illustrations were constructed with Prism (7.0; GraphPad Software). Pilot studies to determine the variability of outcome measures and the effective size were used to estimate the number of observations necessary to test the null hypothesis. All graphical representations display the mean of the observations in a group with bar graphs and the error bars depicting SEM. Distribution-free statistical analyses were performed in Prism using the nonparametric Mann–Whitney rank comparison. The cutoff for significance was *, $P < 0.05$. The rhythm amplitude of the daily ISF Aβ oscillation was determined using the circadian cosinor method (Cosinor Software). A cosine transformation was applied to the time variable with 24 h circadian cycle for the daily temperature and ISF Aβ oscillation (nonlinear regression equation: y = baseline + amplitude * cos((frequency * x) + phase shift)) in Prism (Huang et al., 2012).

Online supplemental material

Fig. S1 shows temperature probe data, wheel running actigraphy data, cortical clock gene expression data, and amyloid plaque quantification from 3–4-mo *APPPS1-21* mice, demonstrating that these mice have moderate plaque burden but maintain normal circadian rhythms in both 12-h:12-h L:D and DD conditions and have normal clock gene expression. Fig. S2 contains qPCR data quantifying 13 candidate transcripts known to be involved in Aβ metabolism in both *Nes-Bmal1 KO;APP* and *Bmal1 iKO;APP* mice, revealing up-regulation of *Apoe* in both models.

ACKNOWLEDGMENTS

We thank Risham Singh, Collin Nadarajah, and David Xiong for assistance with animal husbandry and tissue procurement, and we thank Drs. Erik D. Herzog and John R. Cirrito for their expert advice and comments.

Experiments were performed in part through the support of the Hope Center Surgery and Viral Vector Cores at Washington University in St. Louis and the Washington University in St. Louis Center for Cellular Imaging. This work is supported by a National Institute on Aging grant K01AG053425 (G.J. Kress), National Institute on Neurological Disorders and Stroke grants K08NS079405 (E.S. Musiek) and P01NS074969 (D.M. Holtzman), an Alzheimer's Association New Investigator Research Grant (E.S. Musiek), and the Donors Cure Foundation (E.S. Musiek).

The authors declare no competing financial interests.

Author contributions: G.J. Kress conducted the experiments, injections, surgeries, microdialysis, Aβ assays, data analysis, and imaging. E.S. Musiek developed the mouse lines and assisted with immunohistochemistry, qPCR, and imaging. F. Liao provided technical expertise with microdialysis and Aβ assays. J. Dimitry conducted the qPCR transcript analysis. M.R. Cedeno assisted with mouse breeding and immunohistochemistry. G.J. Kress, E.S. Musiek, and D.M. Holtzman designed the experiments. G.A. FitzGerald provided the original *Nestin-Cre^{+}: Bmal1$^{f/f}$* and *CAG-Cre^{ERT2}:Bmal1(f/f)* mice. G.J. Kress and E.S. Musiek prepared the manuscript with editorial assistance from D.M. Holtzman.

Submitted: 24 December 2017

Revised: 22 January 2018

Accepted: 25 January 2018

REFERENCES

Bunger, M.K., L.D. Wilsbacher, S.M. Moran, C. Clendenin, L.A. Radcliffe, J.B. Hogenesch, M.C. Simon, J.S. Takahashi, and C.A. Bradfield. 2000. Mop3 is an essential component of the master circadian pacemaker in mammals. *Cell*. 103:1009–1017. https://doi.org/10.1016/S0092-8674(00)00205-1

Chen, Q., X.D. Peng, C.Q. Huang, X.Y. Hu, and X.M. Zhang. 2015. Association between ARNTL (BMAL1) rs2278749 polymorphism T >C and susceptibility to Alzheimer disease in a Chinese population. *Genet. Mol. Res.* 14:18515–18522. https://doi.org/10.4238/2015.December.23.39

Cirrito, J.R., P.C. May, M.A. O'Dell, J.W. Taylor, M. Parsadanian, J.W. Cramer, J.E. Audia, J.S. Nissen, K.R. Bales, S.M. Paul, et al. 2003. In vivo assessment of brain interstitial fluid with microdialysis reveals plaque-associated changes in amyloid-beta metabolism and half-life. *J. Neurosci.* 23:8844–8853.

Cronin, P., M.J. McCarthy, A.S.P. Lim, D.P. Salmon, D. Galasko, E. Masliah, P.L. De Jager, D.A. Bennett, and P. Desplats. 2017. Circadian alterations during early stages of Alzheimer's disease are associated with aberrant cycles of DNA methylation in BMAL1. *Alzheimers Dement.* 13:689–700. https://doi.org/10.1016/j.jalz.2016.10.003

DeMattos, R.B., J.R. Cirrito, M. Parsadanian, P.C. May, M.A. O'Dell, J.W. Taylor, J.A. Harmony, B.J. Aronow, K.R. Bales, S.M. Paul, and D.M. Holtzman. 2004. ApoE and clusterin cooperatively suppress Abeta levels and deposition: Evidence that ApoE regulates extracellular Abeta metabolism in vivo. *Neuron*. 41:193–202. https://doi.org/10.1016/S0896-6273(03)00850-X

Fagan, A.M., M. Watson, M. Parsadanian, K.R. Bales, S.M. Paul, and D.M. Holtzman. 2002. Human and murine ApoE markedly alters A beta metabolism before and after plaque formation in a mouse model of Alzheimer's disease. *Neurobiol. Dis.* 9:305–318. https://doi.org/10.1006/nbdi.2002.0483

Harper, D.G., L. Volicer, E.G. Stopa, A.C. McKee, M. Nitta, and A. Satlin. 2005. Disturbance of endogenous circadian rhythm in aging and Alzheimer disease. *Am. J. Geriatr. Psychiatry.* 13:359–368. https://doi.org/10.1097/00019442-200505000-00004

Harper, D.G., E.G. Stopa, V. Kuo-Leblanc, A.C. McKee, K. Asayama, L. Volicer, N. Kowall, and A. Satlin. 2008. Dorsomedial SCN neuronal

subpopulations subserve different functions in human dementia. *Brain*. 131:1609–1617. https://doi.org/10.1093/brain/awn049

Hastings, M.H., and M. Goedert. 2013. Circadian clocks and neurodegenerative diseases: time to aggregate? *Curr. Opin. Neurobiol.* 23:880–887. https://doi.org/10.1016/j.conb.2013.05.004

Hatfield, C.F., J. Herbert, E.J. van Someren, J.R. Hodges, and M.H. Hastings. 2004. Disrupted daily activity/rest cycles in relation to daily cortisol rhythms of home-dwelling patients with early Alzheimer's dementia. *Brain*. 127:1061–1074. https://doi.org/10.1093/brain/awh129

Holtzman, D.M., A.M. Fagan, B. Mackey, T. Tenkova, L. Sartorius, S.M. Paul, K. Bales, K.H. Ashe, M.C. Irizarry, and B.T. Hyman. 2000. Apolipoprotein E facilitates neuritic and cerebrovascular plaque formation in an Alzheimer's disease model. *Ann. Neurol.* 47:739–747. https://doi.org/10.1002/1531-8249(200006)47:6<739::AID-ANA6>3.0.CO;2-8

Huang, Y., R. Potter, W. Sigurdson, A. Santacruz, S. Shih, Y.E. Ju, T. Kasten, J.C. Morris, M. Mintun, S. Duntley, and R.J. Bateman. 2012. Effects of age and amyloid deposition on Aβ dynamics in the human central nervous system. *Arch. Neurol.* 69:51–58. https://doi.org/10.1001/archneurol.2011.235

Kang, J.E., M.M. Lim, R.J. Bateman, J.J. Lee, L.P. Smyth, J.R. Cirrito, N. Fujiki, S. Nishino, and D.M. Holtzman. 2009. Amyloid-beta dynamics are regulated by orexin and the sleep-wake cycle. *Science.* 326:1005–1007. https://doi.org/10.1126/science.1180962

Kim, J., H. Jiang, S. Park, A.E. Eltorai, F.R. Stewart, H. Yoon, J.M. Basak, M.B. Finn, and D.M. Holtzman. 2011. Haploinsufficiency of human APOE reduces amyloid deposition in a mouse model of amyloid-β amyloidosis. *J. Neurosci.* 31:18007–18012. https://doi.org/10.1523/JNEUROSCI.3773-11.2011

Kress, G.J., N. Yamawaki, D.L. Wokosin, I.R. Wickersham, G.M. Shepherd, and D.J. Surmeier. 2013. Convergent cortical innervation of striatal projection neurons. *Nat. Neurosci.* 16:665–667. https://doi.org/10.1038/nn.3397

Laposky, A., A. Easton, C. Dugovic, J. Walisser, C. Bradfield, and F. Turek. 2005. Deletion of the mammalian circadian clock gene BMAL1/Mop3 alters baseline sleep architecture and the response to sleep deprivation. *Sleep.* 28:395–410. https://doi.org/10.1093/sleep/28.4.395

Lim, A.S., M. Kowgier, L. Yu, A.S. Buchman, and D.A. Bennett. 2013. Sleep Fragmentation and the Risk of Incident Alzheimer's Disease and Cognitive Decline in Older Persons. *Sleep (Basel).* 36:1027–1032. https://doi.org/10.5665/sleep.2802

Maywood, E.S., J. O'Neill, G.K. Wong, A.B. Reddy, and M.H. Hastings. 2006. Circadian timing in health and disease. *Prog. Brain Res.* 153:253–269. https://doi.org/10.1016/S0079-6123(06)53015-8

Mieda, M., and T. Sakurai. 2011. Bmal1 in the nervous system is essential for normal adaptation of circadian locomotor activity and food intake to periodic feeding. *J. Neurosci.* 31:15391–15396. https://doi.org/10.1523/JNEUROSCI.2801-11.201122031885

Mohawk, J.A., C.B. Green, and J.S. Takahashi. 2012. Central and peripheral circadian clocks in mammals. *Annu. Rev. Neurosci.* 35:445–462. https://doi.org/10.1146/annurev-neuro-060909-153128

Musiek, E.S., and D.M. Holtzman. 2016. Mechanisms linking circadian clocks, sleep, and neurodegeneration. *Science.* 354:1004–1008. https://doi.org/10.1126/science.aah4968

Musiek, E.S., M.M. Lim, G. Yang, A.Q. Bauer, L. Qi, Y. Lee, J.H. Roh, X. Ortiz-Gonzalez, J.T. Dearborn, J.P. Culver, et al. 2013. Circadian clock proteins regulate neuronal redox homeostasis and neurodegeneration. *J. Clin. Invest.* 123:5389–5400. https://doi.org/10.1172/JCI70317

Musiek, E.S., M. Bhimasani, M.A. Zangrilli, J.C. Morris, D.M. Holtzman, and Y.E. Ju. 2018. Circadian Rest-Activity Pattern Changes in Aging and Preclinical Alzheimer Disease. *JAMA Neurol.* In press. https://doi.org/10.1001./jamaneurol.2017.4719

Pilz, L.K., C.L. Quiles, E. Dallegrave, R. Levandovski, M.P. Hidalgo, and E. Elisabetsky. 2015. Differential susceptibility of BALB/c, C57BL/6N, and CF1 mice to photoperiod changes. *Rev. Bras. Psiquiatr.* 37:185–190. https://doi.org/10.1590/1516-4446-2014-1454

Radde, R., T. Bolmont, S.A. Kaeser, J. Coomaraswamy, D. Lindau, L. Stoltze, M.E. Calhoun, F. Jäggi, H. Wolburg, S. Gengler, et al. 2006. Abeta42-driven cerebral amyloidosis in transgenic mice reveals early and robust pathology. *EMBO Rep.* 7:940–946. https://doi.org/10.1038/sj.embor.7400784

Roh, J.H., Y. Huang, A.W. Bero, T. Kasten, F.R. Stewart, R.J. Bateman, and D.M. Holtzman. 2012. Disruption of the sleep-wake cycle and diurnal fluctuation of β-amyloid in mice with Alzheimer's disease pathology. *Sci. Transl. Med.* 4:150ra122. https://doi.org/10.1126/scitranslmed.3004291

Roh, J.H., H. Jiang, M.B. Finn, F.R. Stewart, T.E. Mahan, J.R. Cirrito, A. Heda, B.J. Snider, M. Li, M. Yanagisawa, et al. 2014. Potential role of orexin and sleep modulation in the pathogenesis of Alzheimer's disease. *J. Exp. Med.* 211:2487–2496. https://doi.org/10.1084/jem.20141788

Satlin, A., L. Volicer, E.G. Stopa, and D. Harper. 1995. Circadian locomotor activity and core-body temperature rhythms in Alzheimer's disease. *Neurobiol. Aging.* 16:765–771. https://doi.org/10.1016/0197-4580(95)00059-N

Song, H., M. Moon, H.K. Choe, D.H. Han, C. Jang, A. Kim, S. Cho, K. Kim, and I. Mook-Jung. 2015. Aβ-induced degradation of BMAL1 and CBP leads to circadian rhythm disruption in Alzheimer's disease. *Mol. Neurodegener.* 10:13. https://doi.org/10.1186/s13024-015-0007-x

Storch, K.F., C. Paz, J. Signorovitch, E. Raviola, B. Pawlyk, T. Li, and C.J. Weitz. 2007. Intrinsic circadian clock of the mammalian retina: importance for retinal processing of visual information. *Cell.* 130:730–741. https://doi.org/10.1016/j.cell.2007.06.045

Swaab, D.F., E. Fliers, and T.S. Partiman. 1985. The suprachiasmatic nucleus of the human brain in relation to sex, age and senile dementia. *Brain Res.* 342:37–44. https://doi.org/10.1016/0006-8993(85)91350-2

Toh, K.L., C.R. Jones, Y. He, E.J. Eide, W.A. Hinz, D.M. Virshup, L.J. Ptácek, and Y.H. Fu. 2001. An hPer2 phosphorylation site mutation in familial advanced sleep phase syndrome. *Science.* 291:1040–1043. https://doi.org/10.1126/science.1057499

Tranah, G.J., T. Blackwell, K.L. Stone, S. Ancoli-Israel, M.L. Paudel, K.E. Ensrud, J.A. Cauley, S. Redline, T.A. Hillier, S.R. Cummings, and K. Yaffe. SOF Research Group. 2011. Circadian activity rhythms and risk of incident dementia and mild cognitive impairment in older women. *Ann. Neurol.* 70:722–732. https://doi.org/10.1002/ana.22468

Wang, J.L., A.S. Lim, W.Y. Chiang, W.H. Hsieh, M.T. Lo, J.A. Schneider, A.S. Buchman, D.A. Bennett, K. Hu, and C.B. Saper. 2015. Suprachiasmatic neuron numbers and rest-activity circadian rhythms in older humans. *Ann. Neurol.* 78:317–322. https://doi.org/10.1002/ana.24432

Witting, W., I.H. Kwa, P. Eikelenboom, M. Mirmiran, and D.F. Swaab. 1990. Alterations in the circadian rest-activity rhythm in aging and Alzheimer's disease. *Biol. Psychiatry.* 27:563–572. https://doi.org/10.1016/0006-3223(90)90523-5

Yang, G., Z. Jia, T. Aoyagi, D. McClain, R.M. Mortensen, and T. Yang. 2012. Systemic PPARγ deletion impairs circadian rhythms of behavior and metabolism. *PLoS One.* 7:e38117. https://doi.org/10.1371/journal.pone.0038117

Yang, G., L. Chen, G.R. Grant, G. Paschos, W.L. Song, E.S. Musiek, V. Lee, S.C. McLoughlin, T. Grosser, G. Cotsarelis, and G.A. FitzGerald. 2016. Timing of expression of the core clock gene Bmal1 influences its effects on aging and survival. *Sci. Transl. Med.* 8:324ra16. https://doi.org/10.1126/scitranslmed.aad3305

Yu, E.A., and D.R. Weaver. 2011. Disrupting the circadian clock: gene-specific effects on aging, cancer, and other phenotypes. *Aging (Albany N.Y.).* 3:479–493.

Zhou, J.N., M.A. Hofman, and D.F. Swaab. 1995. VIP neurons in the human SCN in relation to sex, age, and Alzheimer's disease. *Neurobiol. Aging.* 16:571–576. https://doi.org/10.1016/0197-4580(95)00043-E

SUPPLEMENTAL MATERIAL

Kress et al., https://doi.org/10.1084/jem.20172347

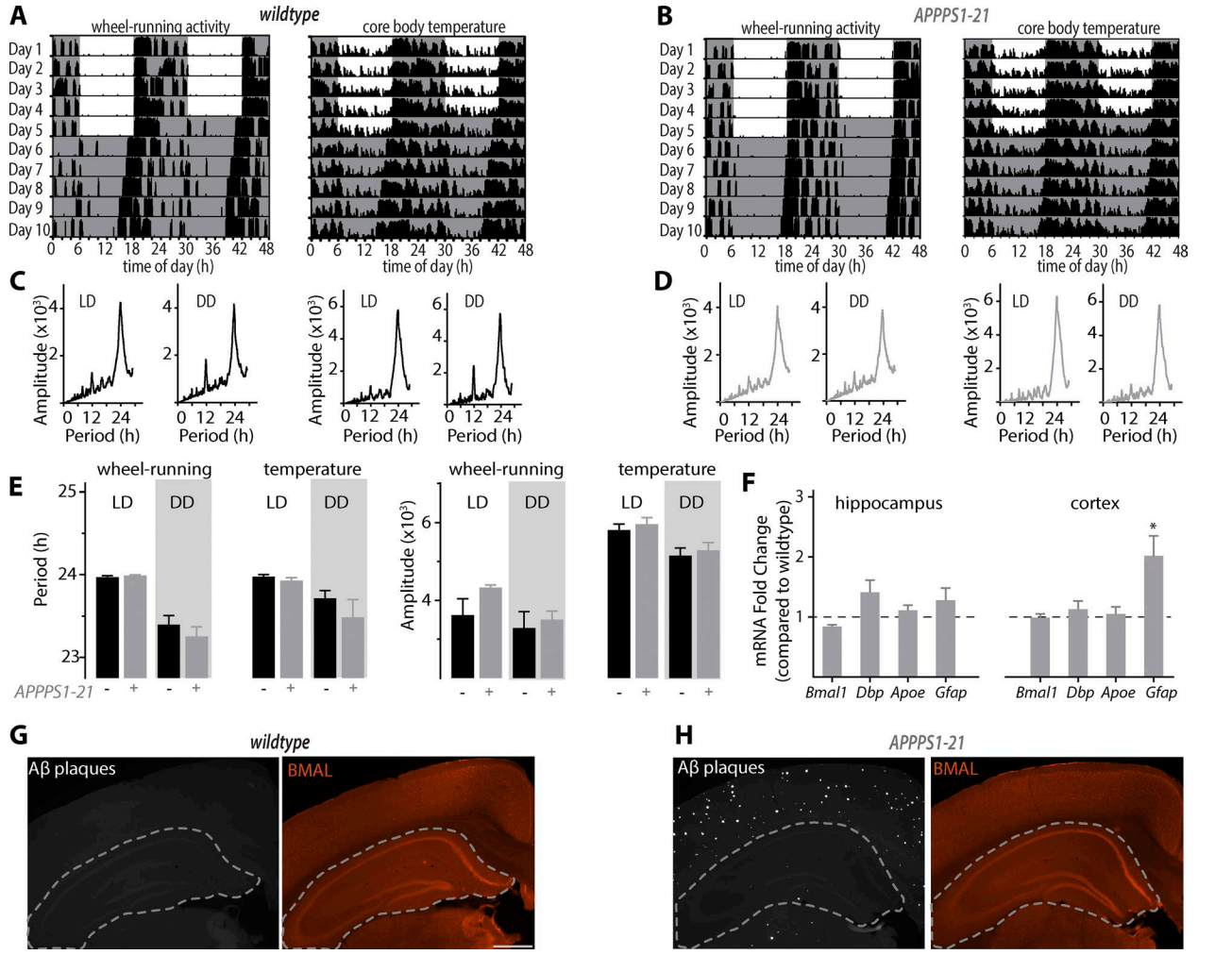

Figure S1. **Behavioral circadian rhythms and the circadian molecular clock are similar in 3–4-mo WT and APPPS1-21 mice. (A)** Representative raw tracing of wheel-running activity (left) and core body temperature recordings (right) over 5 d of 12-h:12-h L:D (shaded gray) followed by 5 d of constant darkness in a 3–4-mo WT mouse. **(B)** Representative raw tracing of wheel running (left) and core body temperature recordings (right) over 5 d of 12-h:12-h L:D followed by 5 d of constant darkness in a 3–4-mo *APPPS1-21* mouse. RU, relative units. **(C)** Representative χ^2 periodograms showing dominant 24-h rhythms in L:D and DD conditions for wheel-running activity and core body temperature oscillations from a 3–4-mo WT mouse. **(D)** Representative χ^2 periodograms showing dominant 24-h rhythms in L:D and DD conditions for wheel-running activity and core body temperature oscillations from a 3–4-mo *APPPS1-21* mouse (gray). **(E)** Mean χ^2 analysis period and amplitude for wheel running and core body temperature in 3–4-mo WT mice (black bars) and 3–4-mo *APPPS1-21* mice (gray bars; n = 4–5 mice per genotype) in L:D and DD (shaded gray). Means were NS by two-tailed t tests (WT compared with *APPPS1-21* for the χ^2 periods left to right: P = 0.40, 0.46, 0.44, and 0.47; for the χ^2 amplitudes left to right: P = 0.29, 0.73, 0.62, and 0.59). **(F)** mRNA transcript analysis of circadian genes *Bmal1* and *Dbp*, APP processing-related gene *Apoe*, and astrogliosis were evaluated from hippocampal (left) and cortical (right) tissue. Gray bars represent mean mRNA levels from 3–4-mo *APPPS1-21* tissue expressed as a fold change compared with WT tissue (gray dotted line), and whiskers represent SEM. n = 3–5 mice per genotype. Means were NS by two-tailed t tests other than cortical *Gfap* levels (hippocampal WT compared with hippocampal *APPPS1-21* left to right: P = 0.14, 0.39, 0.57, and 0.25; cortical WT compared with cortical *APPPS1-21* left to right: P = 0.57, 0.57, 0.99, and 0.036). *, P < 0.05 by two-tailed t test. **(G)** Representative images from a 3–4-mo WT mouse show no fibrillar Aβ plaques within the hippocampus or cortex (left) and normal BMAL1 protein level (right). The hippocampus is outlined by dashed gray lines. **(H)** Representative images from a 3–4-mo *APPPS1-21* mouse show fibrillar Aβ plaques within the hippocampus and cortex (left) and normal BMAL protein levels (right). The hippocampus is outlined by dashed gray lines. Bars, 500 µm.

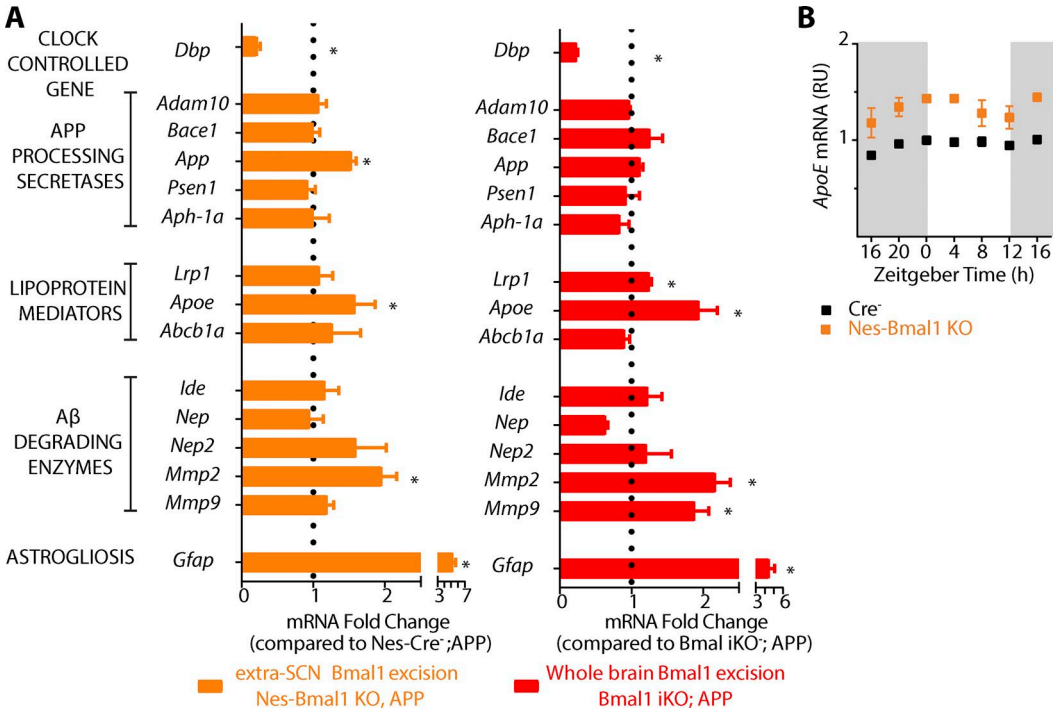

Figure S2. **mRNA transcript analysis. (A)** mRNA transcript analysis of circadian clock–controlled gene, *Dbp*, APP processing–related secretases, lipoprotein mediators, Aβ-degrading enzymes, and astrogliosis were evaluated from the cortex of 4-mo *Nes-Bmal KO; APP* (orange) and 4-mo *Bmal iKO; APP* (red) mice. Bars represent mean mRNA levels expressed as a fold change compared with *Cre*$^{-}$*; APP* tissue (black dotted line), and whiskers represent SEM. n = 5–6 mice per genotype. Means were NS by two-tailed t test other than when indicated with *, $P < 0.05$. (*Cre*$^{-}$*; APP* compared with *Nes-Bmal KO; APP* top to bottom P = 0.002, 0.48, 0.39, 0.04, 0.48, 0.76, 0.82, 0.04, 0.93, 0.93, 0.99, 0.48, 0.002, 0.31, and 0.004; tamoxifen-treated *Cre*$^{-}$*; APP* compared with *Bmal iKO; APP* top to bottom P = 0.004, 0.66, 0.18, 0.08, 0.79, 0.43, 0.03, 0.03, 0.54, 0.39, 0.36, 0.90, 0.01, 0.004, and 0.002.) **(B)** *Apoe* levels were statically elevated in *Nes-Bmal1 KO* mice (orange) compared with WT mice (black) over a 24-h period. Bars represent mean mRNA levels expressed as a fold change compared with WT levels at Zeitgeber time = 0, and whiskers represent SEM. n = 2–4 mice per genotype per time point.